

Design of Multi-Input Multi-Output Systems Based on Low-Density Parity-Check Codes

Jilei Hou, *Member, IEEE*, Paul H. Siegel, *Fellow, IEEE*, and Laurence B. Milstein, *Fellow, IEEE*

Abstract—We design serial concatenated multi-input multi-output systems based on low-density parity-check (LDPC) codes. We employ a receiver structure combining the demapper/detector and the decoder in an iterative fashion. We consider the *a posteriori* probability (APP) demapper, as well as a suboptimal demapper incorporating interference cancellation with linear filtering. Extrinsic information transfer (EXIT) chart analysis is applied to study the convergence behavior of the proposed schemes. We show that EXIT charts match very well with the simulated decoding trajectories, and they help explain the impact of different mappings and different demappers. It is observed that if the APP demapper transfer characteristics are almost flat, the LDPC codes optimized for binary-input channels are good enough to achieve performance close to the channel capacity. We also present a simple code-optimization method based on EXIT chart analysis, and we design a rate-1/2 LDPC code that achieves very low bit-error rates within 0.15 dB of the capacity of a two-input two-output Rayleigh fading channel with 4-pulse amplitude modulation. We next propose to use a space-time block code as an inner code of our serial concatenated coding scheme. By means of a simple example scheme, using an Alamouti inner code, we demonstrate that the design/optimization of the outer code (e.g., LDPC code) is greatly simplified.

Index Terms—Alamouti code, extrinsic information transfer (EXIT) chart, low-density parity-check (LDPC) codes, multi-input multi-output (MIMO) channels, space-time block codes (STBCs).

I. INTRODUCTION

RECENT research progress in information theory has shown that large gains in capacity and reliability of communications over wireless fading channels are possible by exploiting spatial diversity with the use of multiple transmit and receive antennas [1]. Approaching the capacity of such multi-input multi-output (MIMO) channels requires a very good channel code to overcome time-varying fading, intersymbol interference, and noise. Recently, simple but effective space-time transmission schemes consisting of a serial concatenation of a channel encoder, a bit-wise interleaver, and

a spatial constellation mapper have been studied [2]–[6]. These schemes, involving the turbo principle [7], combine the demapper/detector and the decoder in an iterative fashion to approximate the optimal joint demapper and the decoder. The channel codes used are binary convolutional codes or turbo codes. More sophisticated schemes based on space-time turbo trellis-coded modulations [8], [9] have been considered where the constituent codes are trellis codes. Furthermore, serial concatenation schemes using space-time trellis codes [9] or space-time block codes (STBCs) [10] as inner codes have also been proposed. An excellent survey of the related work is provided in [8]. We note that the performance of these systems has been evaluated primarily by computer simulations.

Extrinsic information transfer (EXIT) charts [11], [12] have been shown to be versatile analytical tools for studying the convergence behavior, particularly in the turbo cliff region [11], of iterative receivers for various serial or parallel concatenated systems. The charts have been used to help understand the behavior of the iterative decoding algorithms and to select different codes, typically convolutional codes, to optimize the system performance. In particular, turbo-coded MIMO systems have recently been analyzed in [13] by using the EXIT chart approach.

On the other hand, several research groups have proposed different versions of low-density parity-check (LDPC) code design for high-order constellations on single-input single-output (SISO) channels to achieve bandwidth efficiency, e.g., based on multilevel coding (MLC) [14]–[16] or bit-interleaved coded modulation (BICM) [17], [18] schemes. In this paper, we propose a serial concatenated LDPC-coded MIMO system [19]. For the iterative receiver, we consider an *a posteriori* probability (APP) demapper [4], as well as a suboptimal demapper consisting of a parallel interference canceler (PIC) followed by a minimum mean-square error (MMSE) filter. The latter demapper is analogous to the multiuser detector proposed in [20]. The system performance is analyzed and optimized based on EXIT charts. We prove that, under the assumption of perfect *a priori* information, the APP demapper and the PIC-MMSE demapper are equivalent, as confirmed by the EXIT chart results. Simultaneously with our work, [21] independently used EXIT charts to study LDPC-coded MIMO systems. The key difference between these two approaches is that in the EXIT chart analysis, [21] combines the MIMO detector and bit nodes of the LDPC decoder into one component for the EXIT curve analysis and treats the check-node decoder as the other. In contrast, we treat the MIMO detector as one component for the EXIT curve analysis, and the entire LDPC decoder (including both bit-node and check-node decoders) as the other. The way we divide the system gives us a clear view of

Paper approved by A. H. Banihashemi, the Editor for Coding and Communication Theory of the IEEE Communications Society. Manuscript received April 23, 2003; revised June 16, 2004; October 1, 2004. This work was supported in part by the Center for Wireless Communications of UCSD and the CoRe program of the State of California. This paper was presented in part at the 40th Annual Allerton Conference on Communication, Control, and Computing, Monticello, IL, Oct. 2002.

J. Hou was with the Department of Electrical and Computer Engineering, University of California, San Diego, La Jolla, CA 92093 USA. He is now with the Corporate R&D Group, Qualcomm, Inc., San Diego, CA 92121 USA (jhou@qualcomm.com).

P. H. Siegel and L. B. Milstein are with the Department of Electrical and Computer Engineering, University of California, San Diego, La Jolla, CA 92093 USA (psiegel@ucsd.edu; milstein@ece.ucsd.edu).

Digital Object Identifier 10.1109/TCOMM.2005.844972

the separate effects of the code and the mapper, since we can study the slope and shape of the demapper transfer curves and the decoder transfer curves separately. However, for the same scheme setup, we believe that these two approaches should produce optimized codes with very comparable performance, if not exactly the same. This approach also makes it amenable if we would like to introduce some inner codes to change the shape of the demapper transfer curves, as we discuss later.

To obtain capacity-approaching performance, we present a simple code-optimization method for LDPC codes based on EXIT chart analysis. This optimization method is independently proposed in [22] for application to turbo-coded systems on a SISO channel. For the LDPC decoding algorithms, we can either reset the check-node messages or retain them after each demapper-decoder loop iteration. The analysis and optimization in the paper rely on the use of resetting algorithms. However, our experimental results show that the nonresetting algorithms achieve at least the same performance as the resetting algorithms, and usually converge faster. Therefore, they may be of more practical importance. We demonstrate that the optimized LDPC codes achieve reliable transmission within 0.15 dB of the capacity of a MIMO Rayleigh fading channel, assuming independent and identically distributed (i.i.d.) equiprobable inputs.

STBCs [23], [24] have been introduced to achieve spatial diversity. Due to the orthogonal structure of the STBCs, the symbols transmitted simultaneously from different antennas can be separated at the receiver by simple linear combining, which suggests that by using an STBC code, a MIMO channel is transformed into a SISO channel [25], [26]. Motivated by this result and some observations from our EXIT chart analysis, we revisit the serial concatenated coding scheme using an STBC code as an inner code. By a simple example based on the Alamouti code [23], we demonstrate why this architecture greatly simplifies the design/optimization of the outer codes (e.g., LDPC codes). Some tradeoffs associated with this scheme are briefly discussed.

II. SYSTEM ARCHITECTURE

A. Signal Model

We consider a serial concatenated LDPC-coded MIMO system with N_t transmit antennas and N_r receive antennas. The information source is encoded by a rate- r_c LDPC encoder. The coded bits are interleaved bit-wise and grouped into vectors of $N \triangleq mN_t$ address bits $\mathbf{c} = [c_0, \dots, c_{N-1}]$. The mapping device maps each coded binary vector into a length- N_t symbol vector \mathbf{x} with its entries chosen from a constellation A , where $|A| = 2^m$. The channel output vector \mathbf{y} is given by

$$\mathbf{y} = \mathbf{H}\mathbf{x} + \mathbf{n} \quad (1)$$

where \mathbf{H} is an $N_r \times N_t$ channel matrix which has i.i.d. complex Gaussian entries with zero mean and unit variance, and \mathbf{n} represents a length- N_r complex additive white Gaussian noise (AWGN) vector with covariance matrix¹ $E[\mathbf{nn}^*] = 2\sigma^2\mathbf{I}_{N_r}$. The system spectral efficiency is $r_c m N_t$. We assume that the fading coefficients are perfectly known at the receiver.

¹Here * denotes the conjugate transpose of a vector or a matrix.

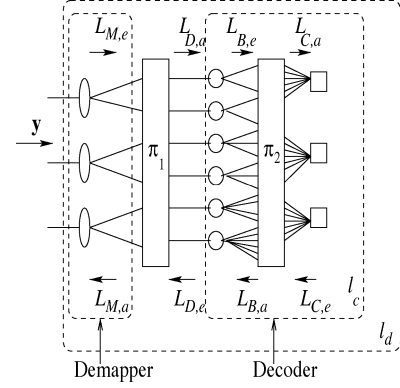


Fig. 1. Iterative demapper/decoder graph.

We apply the turbo principle to decode the received signals. This effectively decomposes the receiver into separate soft-input soft-output components that exchange extrinsic information iteratively. An iterative demapper/decoder graph is illustrated in Fig. 1. There are two levels of iterations involved. One is the demapper-decoder loop including both the demapper and decoder; the other is the decoder loop within the decoder only. For each demapper-decoder loop iteration, the demapper accepts as its inputs \mathbf{y} and *a priori* information $L_{M,a}$ of the coded bits c , and produces extrinsic information $L_{M,e}$. The LDPC decoder accepts *a priori* input $L_{D,a}$, a deinterleaved version of $L_{M,e}$, and performs the sum-product decoding algorithm [27] for l_c decoder-loop iterations, generating the extrinsic output $L_{D,e}$. Then, $L_{D,e}$ is interleaved to become $L_{M,a}$ for the next demapper-decoder loop iteration. The maximum allowable number of demapper-decoder loop iterations is denoted by l_d .

B. Iterative Channel Demapper

1) *APP Demapper*: At the receiver side, the APP demapper computes the extrinsic information for each coded bit c_i , $i = 0, \dots, N - 1$, conditioned on the vector channel output \mathbf{y} , as follows [4]:

$$L_{M,e}(c_i) = \log \frac{\sum_{\mathbf{x} \in \mathbf{A}_i^0} p(\mathbf{y}|\mathbf{x}) \exp\left(\sum_{j \in J_{\mathbf{x},i}} L_{M,a}(c_j)\right)}{\sum_{\mathbf{x} \in \mathbf{A}_i^1} p(\mathbf{y}|\mathbf{x}) \exp\left(\sum_{j \in J_{\mathbf{x},i}} L_{M,a}(c_j)\right)} \quad (2)$$

where $L_{M,a}(c_i) = \log(\Pr(c_i = 0)/\Pr(c_i = 1))$ is the *a priori* information, \mathbf{A}_i^b is the set of length- N_t symbol vectors with $c_i = b$, $b \in \{0, 1\}$, and $J_{\mathbf{x},i}$ is the set of indexes within symbol vector \mathbf{x} with $c_j = 0$, $j = 0, 1, \dots, N - 1$, $j \neq i$. We assume that the coded bits are independent with respect to each other.² Here $p(\mathbf{y}|\mathbf{x})$ is a multivariate Gaussian density function.

The computational complexity of (2) is exponential in $N = mN_t$, becoming prohibitive when N_t gets large. As an alternative, we consider a suboptimal demapper based on soft interference cancellation and linear MMSE filtering whose complexity is proportional to the cube of N_t due to the matrix inversion operations. Therefore, the suboptimal demapper has lower complexity for medium-to-large N_t .

²This assumption is also used for (3).

2) *PIC-MMSE Demapper*: Based on the *a priori* information of the coded bits, $L_{M,a}(c_i)$, $i = 0, \dots, N-1$, we first compute the soft estimates of all the symbols within transmitted vector \mathbf{x} , i.e., for $k = 0, \dots, N_t-1$, $\bar{x}_k = E[x_k] = \sum_{j=0}^{2^m-1} a_j \Pr(x_k = a_j)$, where $A = \{a_j | j = 0, \dots, 2^m-1\}$. Note that

$$\Pr(x_k = a_j) = \prod_{n=0}^{m-1} \Pr(c_{k^*m+n} = a_{j,n}) \quad (3)$$

where

$$\Pr(c_i = b) = \exp\left(\frac{(1-b) \cdot L_{M,a}(c_i)}{(1 + \exp(L_{M,a}(c_i)))}\right)$$

and $a_{j,n}$ denotes the n th index bit of symbol a_j .

We now define $\bar{\mathbf{x}} = [\bar{x}_0, \dots, \bar{x}_{N_t-1}]$ and $\bar{\mathbf{x}}_k = [\bar{x}_0, \dots, \bar{x}_{k-1}, 0, \bar{x}_{k+1}, \dots, \bar{x}_{N_t-1}]$. For each symbol k , a soft interference cancellation is performed on the vector channel output \mathbf{y} , and we obtain

$$\mathbf{y}_k = \mathbf{y} - \mathbf{H}\bar{\mathbf{x}}_k. \quad (4)$$

Next, an MMSE filter is applied to each \mathbf{y}_k to further suppress the residual interference plus noise, i.e., $s_k = \mathbf{w}_k^* \mathbf{y}_k$. Here \mathbf{w}_k is chosen to minimize the mean square error between the symbol x_k and the filter output s_k , and, as in [20], we have

$$\begin{aligned} \mathbf{w}_k &= E[\mathbf{y}_k \mathbf{y}_k^*]^{-1} E[\mathbf{y}_k x_k^*] \\ &= \left(\mathbf{h}_k \mathbf{h}_k^* + \sum_{j \neq k} \frac{E|x_j|^2 - |\bar{x}_j|^2}{E|x_k|^2} \mathbf{h}_j \mathbf{h}_j^* + \frac{2\sigma^2}{E|x_k|^2} \mathbf{I} \right)^{-1} \mathbf{h}_k \end{aligned} \quad (5)$$

where \mathbf{h}_k is the k th column of \mathbf{H} and $E|x_k|^2 = \sum_{j=0}^{2^m-1} |a_j|^2 \Pr(x_k = a_j)$. Following [20], we assume that s_k is the output of an equivalent AWGN channel with x_k as its input, i.e., $s_k = \alpha_k x_k + \lambda_k$, where $\alpha_k = E[s_k x_k^*] / E[x_k x_k^*] = \mathbf{w}_k^* \mathbf{h}_k$, and λ_k is a zero-mean Gaussian random variable with variance $\sigma_k^2 = E|s_k - \alpha_k x_k|^2 = E|x_k|^2 (\alpha_k - |\alpha_k|^2)$. Then, the extrinsic information of each coded bit is given by an expression similar to (2) with \mathbf{y} and \mathbf{x} replaced by s_k and x , respectively.

C. Iterative LDPC Decoder

For the LDPC decoder, we adopt the standard sum-product algorithm, which is summarized as follows. We first consider the message passing from a bit node to its incident d_v check nodes. Given the *a priori* information from the demapper $L_{D,a}$ and the messages from the incident check nodes, for $i = 0, \dots, d_v-1$, the decoder computes $L_{B,e}^i = L_{D,a} + \sum_{j=0, j \neq i}^{d_v-1} L_{B,a}^j$, where $L_{B,a}$ is set to zero at $l_d = 1$ (the first iteration for the demapper-decoder loop). Next we consider the message passing from a check node to its incident d_c bit nodes. The rule for the message updating is $\tanh(L_{C,e}^i/2) = \prod_{j=0, j \neq i}^{d_c-1} \tanh(L_{C,a}^j/2)$, where $L_{C,a}$ is the interleaved version of $L_{B,e}$. The vector $L_{C,e}$ is deinterleaved to become $L_{B,a}$. We can repeat the bit/check message updates for l_c decoder-loop iterations and output the extrinsic information $L_{D,e}$, given by $L_{D,e} = \sum_{j=0}^{d_v-1} L_{B,a}^j$. After $L_{D,e}$ is generated, we can either keep $L_{B,a}$ for the next demapper-decoder loop iteration or reset $L_{B,a}$ to zero. In general, resetting

$L_{B,a}$ results in slower convergence and even performance loss for small l_c . In the nonresetting case, however, the value of l_c has little effect on the performance.

III. EXIT CHART ANALYSIS

We first determine the mutual information (MI) transfer characteristics of the demapper. Following [11], we model the *a priori* input $L_{M,a}$ as a conditional Gaussian random variable with probability density function (pdf) $p_{L_{M,a}}(l|c) = \phi_{\mu_{L_{M,a}}(1-2c), \sigma_{L_{M,a}}^2}(l)$, where $\mu_{L_{M,a}} = \sigma_{L_{M,a}}^2/2$. The MI between c and $L_{M,a}$, denoted $I_{L_{M,a}}$, is defined in [11]. The MI between c and extrinsic information $L_{M,e}$, denoted $I_{L_{M,e}}$, can be computed the same way as $I_{L_{M,a}}$, but with the pdf of $L_{M,e}$. In general, the pdf of $L_{M,e}$ can be determined by Monte Carlo simulation. Viewing $I_{L_{M,e}}$ as a function of $I_{L_{M,a}}$ and the E_b/N_0 (in decibels) of the channel, the demapper EXIT characteristic is given by $I_{L_{M,e}} = T_M(I_{L_{M,a}}, E_b/N_0)$.

Similarly, in the decoder, if we assume that $L_{D,a}$ is Gaussian distributed and we apply the same equations as in the case of the demapper, we can obtain $I_{L_{D,a}}$ and $I_{L_{D,e}}$ from the pdf of $L_{D,a}$ and $L_{D,e}$. However, to make the EXIT chart analysis feasible, $I_{L_{D,e}}$ needs to depend only on $I_{L_{D,a}}$. Therefore, we reset $L_{B,a}$ after each demapper-decoder loop iteration in the decoder. The decoder EXIT characteristic is defined as $I_{L_{D,e}} = T_D(I_{L_{D,a}})$.

In the calculation of $I_{L_{D,e}}$, the pdf of $L_{D,e}$ is determined numerically by density evolution [27], given the pdf of $L_{D,a}$. We recall that an LDPC code ensemble is described by its degree distribution pair (λ, ρ) [27], with $\lambda(x) = \sum_{i=1}^{d_v^{\max}} \lambda_i x^{i-1}$ and $\rho(x) = \sum_{i=1}^{d_c^{\max}} \rho_i x^{i-1}$, where λ_i (resp., ρ_i) is the fraction of edges with bit (resp. check) degree i . Denote $\lambda(p) = \sum_{i=1}^{d_v^{\max}} \lambda_i \otimes^{i-1} p$, $L(p) = \sum_{i=1}^{d_v^{\max}} L_i \otimes^i p$, and $\rho(p) = \Gamma^{-1}(\sum_{i=1}^{d_c^{\max}} \rho_i \otimes^{i-1} \Gamma(p))$, where p is a pdf function, $\{L_i\}$ is the bit degree distribution from the node perspective, \otimes represents convolution, and Γ/Γ^{-1} are density operators defined in [27]. We determine $p_{L_{D,e}}$ as follows. For $1 \leq l \leq l_c$, repeat $p_{L_{B,a}}^{(l)} = \rho(p_{L_{D,a}} \otimes \lambda(p_{L_{B,a}}^{(l-1)}))$, where $p_{L_{B,a}}^{(0)}$ has all mass at zero and l denotes the current decoder-loop iteration number; then, set $p_{L_{D,e}} = L(p_{L_{B,a}}^{(l_c)})$.

A. SISO Systems

We first consider a SISO AWGN channel, which we view as a special case of the MIMO channel. Throughout the paper, we fix the component binary code rate at 1/2 for illustrative purposes. Following the method described above, we obtain the decoder EXIT characteristics for the regular (3,6) LDPC code, decoded with different l_c , shown in Fig. 2. We take two approaches to calculate the pdf of $L_{D,e}$: one is by using density evolution directly, and the other is by running Monte Carlo simulation on a length- 10^6 LDPC code. Both approaches produce virtually the same decoder transfer characteristic curves.

Fig. 3 shows the APP demapper transfer characteristics for 4-pulse amplitude modulation (PAM) on an AWGN channel with three mapping rules used: Gray, natural, and anti-Gray [11]. Different mapping rules appear to generate transfer curves with different slopes. Our results show that on such Gray-mapped SISO channels (either AWGN or fading), the

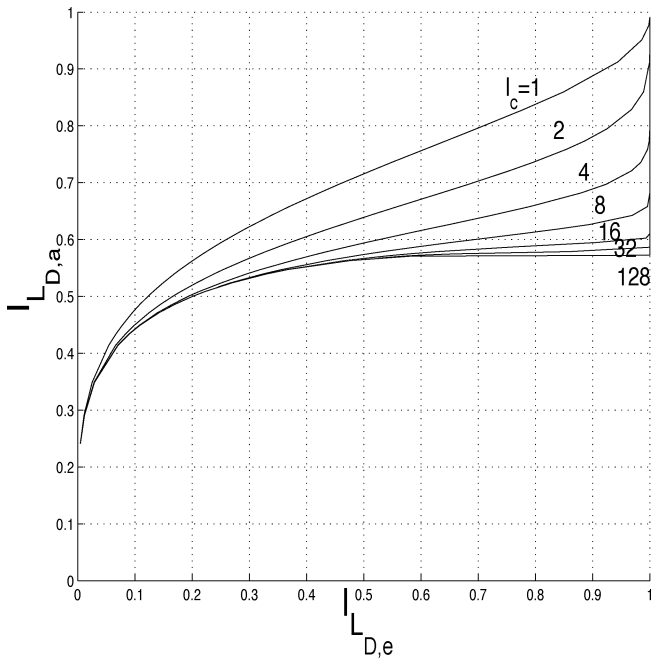


Fig. 2. Decoder transfer characteristics for regular (3,6) LDPC code.

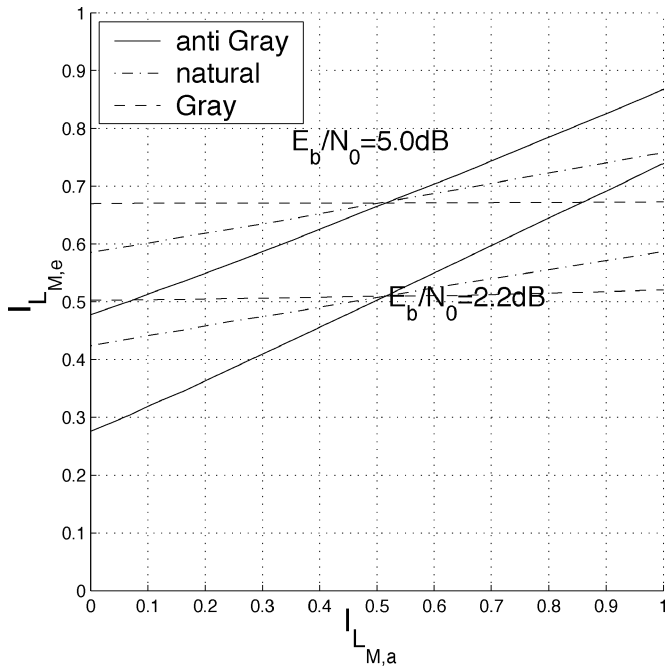


Fig. 3. Demapper transfer characteristics for 4-PAM modulation on an AWGN channel.

demapper curves are almost flat for different high-order constellations [e.g., 8-phase-shift keying (PSK) and 16-quadrature amplitude modulation (QAM)]. This suggests that iterating back to the demapper helps very little to improve the system performance.

If we place the demapper and decoder characteristics into a single diagram, the EXIT chart is generated. Fig. 4 shows an EXIT chart for a system with a (3,6) LDPC code, anti-Gray mapping, and 4-PAM modulation, operating at $E_b/N_0 = 5$ dB. The chart corresponds to $l_c = 4$. To verify the accuracy of the

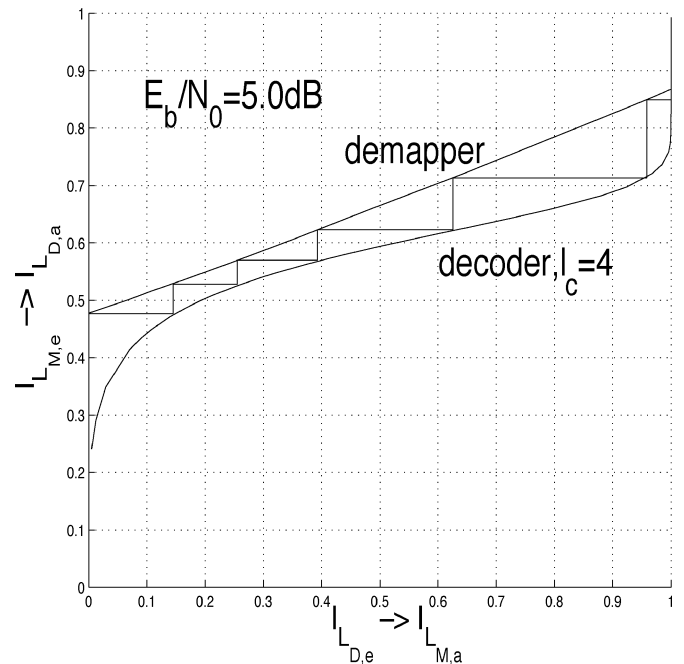


Fig. 4. EXIT chart with iterative decoding trajectory of the anti-Gray mapping, 4-PAM, and (3,6) LDPC code at $E_b/N_0 = 5.0$ dB.

EXIT chart, we show the iterative decoding trajectory based on simulation results for a (3,6) LDPC code of blocksize³ 10^6 . The simulated trajectory matches well with the computed transfer characteristics. Fig. 4 shows that for $l_c = 4$, there is a “tunnel” between the demapper and decoder characteristics that allow the decoding trajectory to continue on to successful decoding.

The smallest E_b/N_0 (dB) at which the iterative scheme converges is referred to as a threshold, or pinch-off limit [11]. The threshold corresponds to the signal-to-noise ratio (SNR) at which the demapper and decoder transfer characteristics are almost tangent and do not cross. For example, the threshold of the iterative scheme with anti-Gray mapping, the (3,6) LDPC code, and $l_c = 32$ is around 4.4 dB. Comparison of the demapper and decoder characteristics in Figs. 2 and 3 shows that the iterative scheme converges at about the same E_b/N_0 when l_c is large (e.g., $l_c \geq 32$). This observation is verified by simulation results.

The results discussed above assume the LDPC decoder is reset after each demapper-decoder loop iteration. However, our simulation results show that if the LDPC decoder is not reset after each demapper-decoder loop iteration, the performance of the iterative scheme is essentially independent of l_c (i.e., $l_c = 1$ is enough), and agrees with that of the resetting decoder for large l_c . These observations apply to a variety of mappings and both SISO and MIMO channels.

The Gaussian input assumption works very well for the demapper transfer-function computation in various cases. For the LDPC decoder transfer-function computation, the Gaussian assumption works well with the anti-Gray mapping on a SISO AWGN channel. For most other cases, this assumption works fine, but produces a discrepancy of about 0.1–0.2 dB between

³In the following, the blocksize for the simulated decoding trajectories are all fixed at 10^6 .

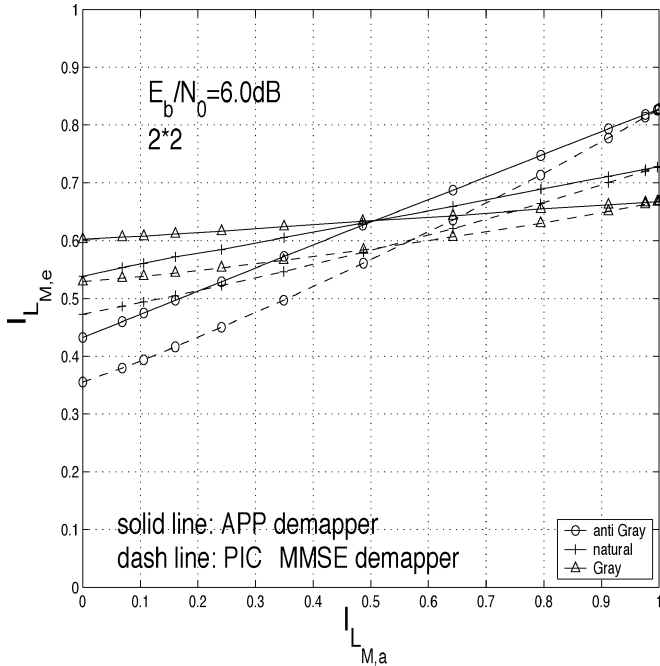


Fig. 5. APP and PIC-MMSE demapper EXIT characteristics of 4-PAM on a 2×2 Rayleigh fading channel.

EXIT charts and real decoding trajectories. In general, this discrepancy is small enough that we may ignore it.

However, we want to have a more accurate model to better match the transfer characteristics of the LDPC decoder to the simulation performance. With the improved accuracy of the modified model, we are better able to optimize the irregular LDPC codes and push the thresholds of the iterative schemes closer toward the channel capacity, as we discuss later.

In the modified model, instead of assuming a Gaussian distribution for the decoder inputs, we assume the decoder inputs are generated by the output of a demapper whose inputs are Gaussian distributed. The motivation for this model is that we believe the output statistics from a demapper (even a very simple one) should approximate the true statistics of a more complicated demapper output better than the simple Gaussian assumption on the demapper output. This intuition is supported by Monte Carlo simulation results. For example, we perform the EXIT chart analysis for the natural mapping and a (3,6) code at $E_b/N_0 = 3.4$ dB on a SISO AWGN channel. The decoder characteristic obtained from the modified model matches well with the simulated trajectory, while the one computed from the original model shows about a 0.1-dB discrepancy. Interestingly, numerous experiments show that for a given LDPC code, the modified model produces virtually the same decoder transfer characteristics for most choices of mappings and channels (SISO or MIMO). Consequently, in the analysis that follows, we will use the modified model with natural mapping on a SISO AWGN channel to compute the decoder transfer characteristics, even though the actual mappings and channels may be different.

B. MIMO Systems

We present results for MIMO systems with $N_t = N_r = 2$. In Fig. 5, we plot both the APP demapper and the PIC-MMSE

TABLE I
THRESHOLDS OF THE (3,6) LDPC-CODED 4-PAM SYSTEMS RELATIVE TO THE I.I.D. CAPACITY WHEN WE CONSIDER DIFFERENT MAPPINGS, DIFFERENT CHANNELS, AND DIFFERENT DEMAPPERS

$(E_b/N_0)_\Delta^*$ (dB)	Gray	natural	anti Gray
SISO AWGN, APP	1.3	1.3	2.3
SISO Rayleigh, APP	1.4	1.4	2.0
2I2O Rayleigh, APP	1.3	1.5	2.5
2I2O Rayleigh, PIC-MMSE	2.2	2.6	4.1

demapper transfer characteristics at $E_b/N_0 = 6.0$ dB. For a given mapping, the PIC-MMSE demapper curve is strictly below the APP demapper curve and tends to have a steeper slope. This result suggests that in comparison with the APP demapper, the PIC-MMSE demapper always suffers information loss. Furthermore, these two curves converge to the same $I_{L,D,e}$ when $I_{L,D,a}$ approaches one. This suggests that with perfect *a priori* information about coded bits c_j , $j = 0, \dots, N-1$, and $j \neq i$, the PIC stage cancels all the interference relative to symbol x_k which contains bit c_i , and the PIC-MMSE solution converges to the APP solution. For both demappers, if we assume perfect *a priori* information, it can be shown that both schemes become single-input multiple-output (SIMO) systems with only two possible inputs. It is straightforward to show that for such a SIMO system, the direct vector-APP detector equals to a scheme of maximum ratio combining (MRC) followed by a symbol-APP detector on the MRC output. On the other, it is known that for such a SIMO system, the MRC combining equals to the MMSE combining [28]. The proof of this fact involves the matrix inversion lemma [29]. Therefore, these two demappers are indeed equivalent, if we have perfect *a priori* information. For more details of the proof, please see the Appendix.

Another interesting phenomenon is that, unlike the SISO case where the APP demapper curve of the Gray mapping is almost flat, in the MIMO case, the corresponding curve has more significant slope. This result suggests that for the Gray-mapped MIMO systems, it is necessary to iterate between demapper and decoder to approach the capacity.

We summarize our threshold results obtained from EXIT chart analysis in Table I, where we show the gaps, $(E_b/N_0)_\Delta^*$ (dB), between the thresholds of the (3,6) LDPC-coded 4-PAM systems and the i.i.d. capacities for the channel models and mappings considered. Note that for 4-PAM, the i.i.d. capacities are 2.11, 3.93, and 3.48 dB for the SISO AWGN, SISO Rayleigh fading, and MIMO (2×2) Rayleigh fading channels, respectively, and the corresponding spectral efficiencies are 1, 1, and 2 b/symbol. Gray and natural mappings have very comparable performance, and are far better than the anti-Gray mapping. For the MIMO Rayleigh fading channel, the PIC-MMSE demapper loses about 0.9~1.6 dB relative to the APP demapper.

IV. CODE OPTIMIZATION

We can see from Table I that the (3,6) LDPC-coded systems are more than 1 dB away from the channel capacities in the various scenarios we have considered. It is natural to ask about the performance attainable with the LDPC codes optimized for the

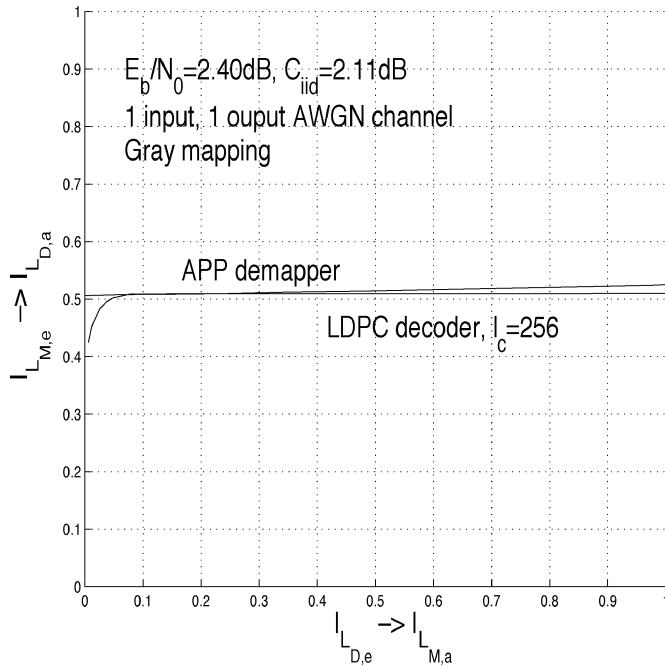


Fig. 6. EXIT chart with iterative decoding trajectories of the systems on a 4-PAM SISO channel with an LDPC code optimized for the binary-input AWGN channel.

binary-input AWGN channel. In Fig. 6, we plot the EXIT charts for 4-PAM systems using a rate-1/2 LDPC code with $d_{v_{\max}} = 50$, designed using the degree distribution pair optimized for the binary-input AWGN channel [27]. The plot is shown for the Gray-mapped SISO channel, where both the demapper and the decoder curves are almost flat and match well with each other, and the threshold of the scheme is about 2.40 dB, which is only 0.29 dB away from the channel capacity (2.11 dB). However, if anti-Gray mapping is used, the slope of the demapper curve is much steeper than the decoder curve, and the scheme does not converge unless the E_b/N_0 is at least 5.10 dB, representing a 3-dB loss relative to the channel capacity. As suggested in [11] and [12], at the threshold SNR value, the area between the two component curves is a measure of the performance loss relative to the channel capacity. Therefore, to optimize the system performance, we need to match these two component curves to minimize the area between them.

For the 4-PAM SISO channel considered above, the APP demapper curves for Gray mapping are almost flat, which means that the parallel independent demapper (PID) introduced in [18] and [30] can nearly achieve the channel capacity. The PID demapper is a special case of the decoding schemes considered here, corresponding to $l_d = 1$. We then consider a rate-1/2 LDPC code optimized for the PID demapper with $d_{v_{\max}} = 50$ from [18]. This code has a threshold of 2.35 dB under the PID demapper. As seen in Fig. 7, at $E_b/N_0 = 2.40$ dB, the “one-shot” process ($l_d = 1$) at the demapper is enough to make the decoding successful, provided l_c is large enough (here we used $l_c = 1024$). Furthermore, if we set $l_c = 256$ and $l_d = 5$, the decoder is able to converge even at $E_b/N_0 = 2.30$ dB. The results suggest that if the demapper transfer curve is very

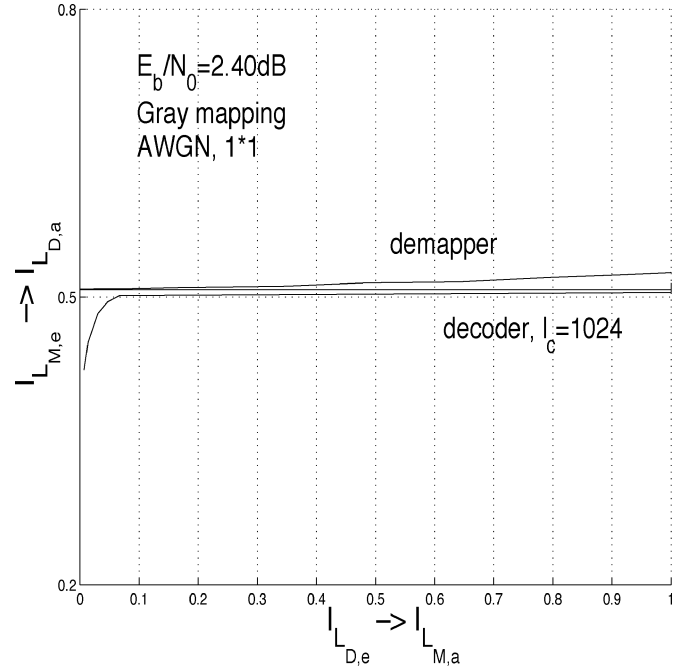


Fig. 7. EXIT chart with iterative decoding trajectories of the Gray mapping and an LDPC code optimized for the PID demapper.

flat, the LDPC codes optimized for binary-input channels⁴ are almost optimal for the iterative decoding schemes.

In general, to optimize the LDPC-coded MIMO systems, we can use a global density-evolution procedure including both the demapper and the decoder. However, it is very difficult to obtain a closed-form solution of the pdf at the output of the demapper, and the Monte Carlo method has computation complexity exponential in N_t for the APP demapper. Therefore, we introduce a simple but effective code-optimization method based on EXIT charts, which was independently proposed in [22]. Unlike the global density-evolution approach, this method does not use error probability as the cost function associated with each degree distribution pair (λ, ρ) . Instead, the cost function is defined as follows. For any LDPC code ensemble, there is a decoder transfer characteristic T_D associated with it. For any given mapping, channel, and demapper, we can compute a demapper-transfer characteristic T_M at a certain E_b/N_0 (dB). Then, on the computed demapper curve, we pick a set of points $I_{L_{M,e}} = \{I_i, i = 0, \dots, o-1\}$, and the cost function is defined as

$$z = \sum_j \left| T_D(I_j) - T_M^{-1} \left(I_j, \frac{E_b}{N_0} \right) \right|^2 \quad (6)$$

where $\{I_j\}$ is the subset of $\{I_i\}$ such that for each I_j , $T_D(I_j) < T_M^{-1}(I_j, E_b/N_0)$. In other words, for each I_j , the decoder curve is on the left side of the demapper curve. The iterative search algorithm proceeds as follows.

- 1) At a certain E_b/N_0 , we compute T_M for the demapper.
- 2) By differential evolution [27], we search for a (λ^*, ρ^*) whose T_D results in the smallest z^* .

⁴As discussed in [18], the coding scheme with the PID demapper has an equivalent binary-input channel-model representation.

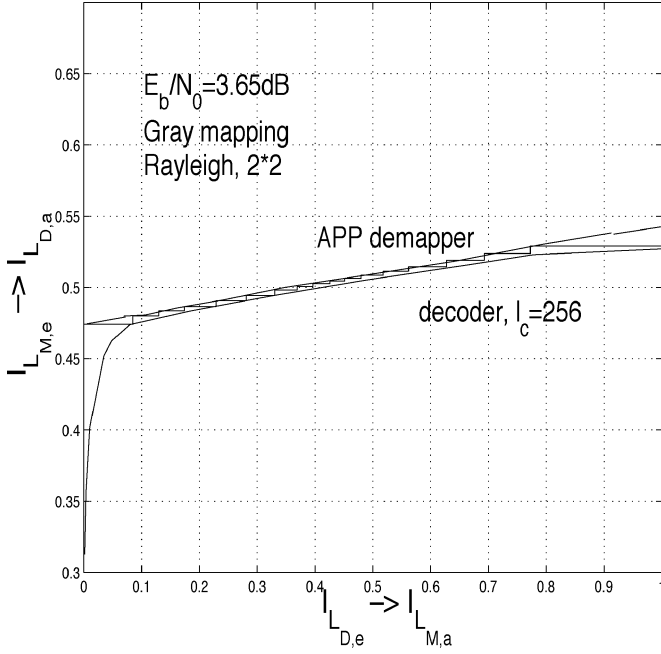


Fig. 8. EXIT chart with iterative decoding trajectories of the Gray mapping and an optimized LDPC code on a 2×2 Rayleigh fading channel, $l_d = 17$.

- 3) If this z^* is smaller than a target z_t , we decrease E_b/N_0 and go back to step 2. If not, we stop.

The optimal degree distribution pair (λ^*, ρ^*) is the pair found in the last iteration with the smallest E_b/N_0 and corresponding cost $z^* < z_t$. In this way, we find a (λ^*, ρ^*) whose T_D is almost on top of the demapper curve T_M . Then, at an E_b/N_0 slightly larger than the E_b/N_0 used in the optimization, there is a narrow, open tunnel between the demapper and the decoder curves, enabling the iterative decoder to converge. Notice that at a specific E_b/N_0 , once T_M is computed, numerous degree sequence pairs generated by differential evolution in step 2 can use the same T_M for their cost-function computations. This translates into significant computational savings when mN_t is large.

In Fig. 8, we show an EXIT chart with iterative decoding trajectories for the LDPC codes optimized for the Gray mapping on a MIMO (2×2) Rayleigh fading channel. The code in the graph is optimized for the APP demapper and the degree distribution pair is given by $\lambda(x) = 0.223095x + 0.264726x^2 + 0.221859x^8 + 0.038578x^{14} + 0.076751x^{29} + 0.174990x^{49}$ and $\rho(x) = 0.390545x^7 + 0.609455x^8$. This degree distribution pair is optimized at $E_b/N_0 = 3.60$ dB, where the demapper curve coincides with the decoder curve over a substantial interval. Then, at $E_b/N_0 = 3.63$ dB and $l_c = 256$, the simulation is able to achieve a low bit-error rate (BER) although the required number of demapper-decoder loop iterations l_d is very large. Note that the corresponding i.i.d. capacity is 3.48 dB. Therefore, the simulation with codeword length 10^6 provides good performance at an E_b/N_0 within 0.15 dB of the i.i.d. capacity. The graph of Fig. 8 shows that at $E_b/N_0 = 3.65$ dB, the decoder is able to converge for a relatively small value of l_d (here $l_d = 17$). On the other hand, we also optimize an LDPC code for the PIC-MMSE demapper, and the degree-distribution pair is described by $\lambda(x) = 0.254218x +$

$0.260964x^2 + 0.126664x^8 + 0.144428x^{14} + 0.213726x^{49}$ and $\rho(x) = 0.714657x^7 + 0.285343x^8$. The degree distribution pair is optimized at $E_b/N_0 = 4.20$ dB, and the simulation shows a high probability of successful decoding at 4.23 dB. Therefore, even with the PIC-MMSE demapper, the proposed scheme is able to achieve reliable transmission within 0.75 dB of the i.i.d. capacity.

Finally, for both codes, the nonresetting receiver with different l_c converges at roughly the same thresholds as does the resetting receiver with large l_c .

V. USING STBCS AS INNER CODES

As shown by the EXIT chart analysis, the mismatch between the demapper curve and the decoder curve usually results in a performance loss relative to the channel capacity. For a given system, at its E_b/N_0 threshold, the larger the area between the demapper and decoder transfer curves on the EXIT chart, the greater the performance loss the system suffers.

We observe that when $N_t > N_r$, even for Gray mapping, the APP demapper curves tend to have steep slopes. The decoder curves of the LDPC codes optimized for the binary-input channels are almost flat in most of the region of interest (see, for example, Fig. 6). Similarly, ten Brink [13] showed that the decoder curves for several known turbo codes are close to flat as well. Therefore, these codes usually do not perform well for the MIMO systems with $N_t > N_r$.

The design methodology presented in the previous section hinges on optimization of the code parameters so that the shape of the decoder curve is matched to the shape of the demapper curve. When $N_t > N_r$ where the demapper curves are very steep, we found that the optimized LDPC codes usually have many more degree-2 nodes, compared with the LDPC codes optimized for the binary-input channels. On the other hand, ten Brink [13] observed that simple convolutional codes can outperform turbo codes in the waterfall region when $N_t > N_r$. However, we observed that, when simulated with small-to-moderate block sizes, the LDPC codes optimized for $N_t > N_r$ normally have high error floors due to the weakness of the component codes. Similar phenomena are visible in [13] for simple convolutional codes as well.

One important observation from the previous section is that, for Gray mapping on a SISO channel, the demapper curves are almost flat, matching well with the decoder curves of the LDPC codes optimized for the binary-input channels, as well as those turbo codes. It is known that, due to the orthogonal structure of the STBC codes, the symbols transmitted simultaneously from different antennas can be separated at the receiver by simple linear combining. Therefore, STBC codes play a key role of transforming a MIMO channel into a SISO channel [25], [26]. In the following, we introduce a serial concatenated scheme when $N_t > N_r$, which uses an STBC code as an inner code and uses an LDPC code optimized for a binary-input channel or a turbo code as an outer code. We demonstrate that, if Gray mapping is employed, this approach flattens the demapper transfer curves. This design method has two important practical features. First, the LDPC code design is greatly simplified; second, simulation

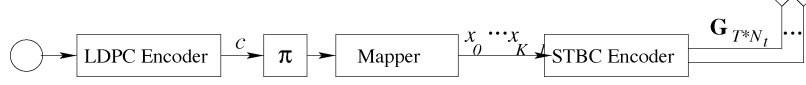


Fig. 9. Coding scheme with an LDPC code as an outer code and an STBC code as an inner code.

results show that, at small-to-moderate block sizes, these codes have no error floors in the BER regions of interest.

Fig. 9 shows a coding scheme using an STBC code as an inner code. The input to the STBC encoder is a block of K complex symbols x_k , $k = 0, \dots, K-1$. The STBC encoder maps the input symbols onto entries of a $T \times N_t$ matrix \mathbf{G} , where T is the number of channel uses required for the transmission of K input symbols and the entries of \mathbf{G} are chosen from $0, \pm x_0, \dots, \pm x_{K-1}, \pm x_0^*, \dots, \pm x_{K-1}^*$, and their linear combinations. Here, we limit the STBC codes to be the complex orthogonal designs introduced in [23] and [24]. The matrix \mathbf{G} satisfies the property $\mathbf{G}^* \mathbf{G} = (|x_0|^2 + \dots + |x_{K-1}|^2) \mathbf{I}$.

The celebrated Alamouti code is a special case of the STBC codes with $T = 2$, $N_t = 2$, $K = 2$, defined by

$$\mathbf{G}_{ac} = \begin{bmatrix} g_{00} & g_{01} \\ g_{10} & g_{11} \end{bmatrix} = \begin{bmatrix} x_0 & x_1 \\ -x_1^* & x_0^* \end{bmatrix}. \quad (7)$$

We assume that the channel coherence time is large compared with T , and therefore, the channel coefficients are constant over the duration of T consecutive channel uses. For $N_r = 1$ (as is commonly the case in downlink transmission for wireless applications), the channel model can be described as

$$\underbrace{\begin{bmatrix} r_0 \\ \vdots \\ r_{T-1} \end{bmatrix}}_{\mathbf{r}} = \mathbf{G} \underbrace{\begin{bmatrix} h_0 \\ \vdots \\ h_{N_t-1} \end{bmatrix}}_{\mathbf{h}} + \underbrace{\begin{bmatrix} n_0 \\ \vdots \\ n_{T-1} \end{bmatrix}}_{\mathbf{n}}. \quad (8)$$

By decoupling the signals transmitted from different antennas, the orthogonality of the columns of \mathbf{G} makes feasible a simple APP decoding technique. It is easy to verify that the APP of x_k , $k = 0, \dots, K-1$, given the received symbols r_0, \dots, r_{T-1} , can be expressed in the following form:

$$\Pr(x_k | r_0, \dots, r_{T-1}) = \text{const} \cdot f_k(x_k) \Pr(x_k) \quad (9)$$

where $f_k(x_k)$ is a function independent of x_i , $i = 0, \dots, K-1$, $i \neq k$. Then, for $k = 0, \dots, K-1$, $n = 0, \dots, m-1$, the log a posteriori probability ratio (LAPPR) of each of the bits can be computed as

$$\begin{aligned} & L_{M,e}(c_{k^*m+n}) \\ &= \log \frac{\Pr(c_{k^*m+n} = 0 | r_0, \dots, r_{T-1})}{\Pr(c_{k^*m+n} = 1 | r_0, \dots, r_{T-1})} - L_{M,a}(c_{k^*m+n}) \\ &= \log \frac{\sum_{x_k \in A_n^0} \Pr(x_k | r_0, \dots, r_{T-1})}{\sum_{x_k \in A_n^1} \Pr(x_k | r_0, \dots, r_{T-1})} - L_{M,a}(c_{k^*m+n}) \\ &= \log \frac{\sum_{x_k \in A_n^0} f_k(x_k) \cdot \exp\left(\sum_{j \in J_{x_k,n}} L_{M,a}(c_{k^*m+j})\right)}{\sum_{x_k \in A_n^1} f_k(x_k) \cdot \exp\left(\sum_{j \in J_{x_k,n}} L_{M,a}(c_{k^*m+j})\right)} \end{aligned} \quad (10)$$

where A_n^b is the set of symbols with $c_{k^*m+n} = b$, and $J_{x_k,n}$ is the set of indexes within symbol x_k with $c_{k^*m+j} = 0$, $j = 0, 1, \dots, m-1$, $j \neq n$. Comparing (2) and (10), we observe that, unlike the spatial multiplexing schemes without STBC inner codes, the extrinsic information update for one bit when using an STBC inner code depends only on the a priori information of the other $m-1$ constituent bits within the symbol x_k , rather than the entire symbol vector \mathbf{x} .

In the case of the Alamouti code, it can be easily verified that

$$\begin{aligned} & f_0(x_0) \\ &= \exp\left(-\frac{(-s_0^* x_0 - s_0 x_0^* + (|h_0|^2 + |h_1|^2) |x_0|^2)}{2\sigma^2}\right) \end{aligned} \quad (11)$$

$$\begin{aligned} & f_1(x_1) \\ &= \exp\left(-\frac{(-s_1^* x_1 - s_1 x_1^* + (|h_0|^2 + |h_1|^2) |x_1|^2)}{2\sigma^2}\right) \end{aligned} \quad (12)$$

where

$$\begin{aligned} s_0 &= h_0^* r_0 + h_1 r_1^* \\ s_1 &= h_1^* r_0 - h_0 r_1^*. \end{aligned} \quad (13)$$

Note that s_0 and s_1 are the outputs of the maximum-likelihood detector described in [23].

For $k = 0, 1$, the normalized equivalent channel model is given as

$$s_k = \sqrt{\frac{|h_0|^2 + |h_1|^2}{2}} x_k + n'_k \quad (14)$$

with $E[n'_k n_k'^*] = 2\sigma^2$ [26]. If we insert a channel interleaver before the STBC encoder and assume ideal channel interleaving at asymptotically large block size, the channel described in (14) becomes a memoryless ergodic channel. We can then compute the capacity of this channel assuming i.i.d. equiprobable inputs.

One example we consider is $N_t = 2$ and $N_r = 1$. We compute the i.i.d. capacity of a channel using 16-QAM with an Alamouti inner code. This scheme has an uncoded transmission rate of 4 b/channel use (uncoded refers to no outer channel coding). At a coded transmission rate of 2 b/channel use, which corresponds to an outer channel code of rate 1/2, the E_b/N_0 required to transmit reliably at the given spectral efficiency is 3.0 dB.

Next, we perform an EXIT chart analysis for the proposed scheme with Alamouti inner code and a rate-1/2 LDPC code optimized for binary-input AWGN channel with $d_{v\max} = 50$ as an outer code, where Gray-mapped 16-QAM is used. The results show that the demapper and decoder curves both are nearly flat and closely aligned. The threshold of this system is about 3.3 dB, which is only 0.3 dB away from the corresponding capacity. With this example, we demonstrate that by using the Alamouti inner code, we greatly simplify the outer code design

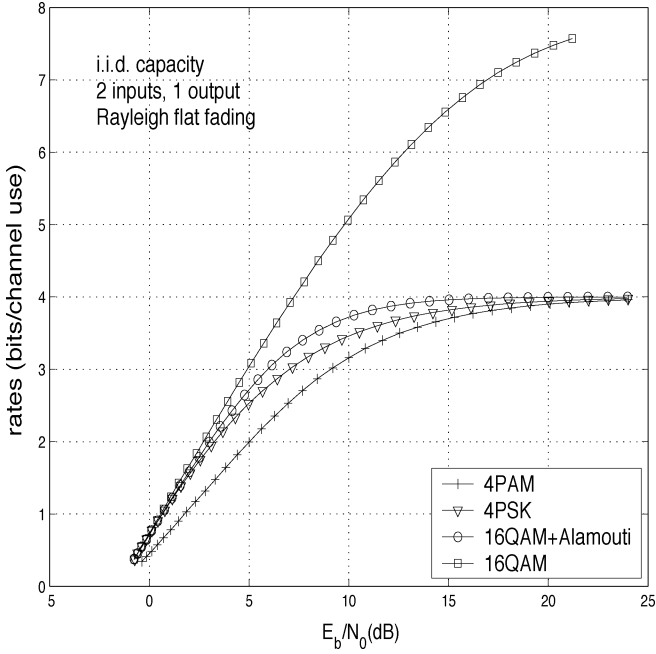


Fig. 10. Capacity comparison of different modulation schemes on a two-input one-output channel assuming uniform finite constrained inputs.

by changing the slope of the demapper curve and aligning it with the decoder curve.

The proposed scheme with the Alamouti inner code essentially transforms a 2×1 channel to an equivalent 1×1 channel specified by (14). It is known that, with continuous Gaussian inputs, the Alamouti code on a 2×1 channel incurs no capacity loss [31]. If we assume finite constrained inputs, similarly we can compute the i.i.d. capacity curves of a 2×1 channel with Alamouti inner code and a 1×1 channel, with 16-QAM. The results are plotted in Fig. 10. We observe that the equivalent channel presented in (14) is still better than the standard 1×1 fading channel. At 2 b/channel use, the 2×1 channel with the Alamouti inner code has about 1-dB advantage over the 1×1 channel. The 2×1 channel with no Alamouti code only achieves an additional 0.3-dB gain at 2 b/channel use, compared with the 2×1 channel with Alamouti code. Furthermore, in a practical system, with the limited interleaver size, a slow-fading channel produces fading coefficients for neighboring symbols that are strongly correlated, and the available time diversity diminishes. In this case, STBC codes still guarantee the spatial diversity. Therefore, our proposed schemes are of practical significance as well.

When $N_t > 2$, we can use the STBC codes introduced in [24] to achieve the same goal as achieved by Alamouti code when $N_t = 2$. However, these codes, in general, require $R_e = K/T < 1$ ($R_e = 1$ for the Alamouti code), and to keep the same transmission spectral efficiency requires constellation expansion by a factor proportional to $1/R_e$. Therefore, as suggested in [21], to compensate for the greater rate loss due to the inner STBC codes, one would have to use a much larger constellation size, making this scheme less appealing when $N_t > 2$. For example, if $N_t = 3$, we can use 4-PSK modulation with the spatial multiplexing scheme to achieve an uncoded transmission rate of 6 b/channel use. If we use an inner STBC code

with $R_e = 3/4$ (see, e.g., [24]), we need to expand the constellation to 256-QAM, to achieve the same transmission rate.

VI. CONCLUSION

We designed a serial concatenated MIMO system based on LDPC codes, and employed a receiver structure that iterates between the demapper and the LDPC decoder. EXIT charts were shown to match very well with simulated decoding trajectories on MIMO channels. We observed that if the APP demapper transfer curve is almost flat, the LDPC codes optimized for the binary-input channels are good enough to achieve performance close to the i.i.d. channel capacity. Furthermore, we proposed a novel code-optimization method if the demapper transfer curve is not flat, and a resulting rate-1/2 irregular code of length 10^6 was shown to achieve a low BER within 0.15 dB of the i.i.d. capacity on a 2×2 MIMO Rayleigh fading channel. Even for the suboptimal PIC-MMSE demapper, the optimized LDPC codes achieve very reliable transmission within 0.75 dB of the i.i.d. channel capacity.

To simplify the LDPC code design, we modified the coding scheme by adding an STBC inner code. Using the Alamouti code ($N_t = 2$), we showed that the demapper transfer curves are nearly flat and align well with the decoder curves of the LDPC codes optimized for the binary-input channels. The corresponding thresholds are quite close to the i.i.d. channel capacity.

APPENDIX

First, we show that with the vector-APP detector, the system can be simplified to a SIMO system if we assume perfect *a priori* information. The APP demapper computes the extrinsic information for each coded bit c_i , $i = 0, \dots, N - 1$, where $N = mN_t$, as

$$L_{M,e}(c_i) = \log \frac{\sum_{\mathbf{x} \in \mathbf{A}_i^0} p(\mathbf{y}|\mathbf{x}) \cdot \prod_{j \neq i} \Pr(c_j)}{\sum_{\mathbf{x} \in \mathbf{A}_i^1} p(\mathbf{y}|\mathbf{x}) \cdot \prod_{j \neq i} \Pr(c_j)}. \quad (15)$$

Since we know perfect information about each coded bit, c_j , $j \neq i$, $\Pr(c_j)$ is either zero or one. Then, in the equation above, within \mathbf{A}_i^0 , there is only one vector \mathbf{x}_i^0 with nonzero product $\prod_{j \neq i} \Pr(c_j) = 1$. So there is only one such \mathbf{x}_i^1 in \mathbf{A}_i^1 . Furthermore, \mathbf{x}_i^0 and \mathbf{x}_i^1 only differ at position i . Therefore, (15) can be simplified as

$$\begin{aligned} L_{M,e}(c_i) &= \log \frac{p(\mathbf{y}|\mathbf{x}_i^0)}{p(\mathbf{y}|\mathbf{x}_i^1)} \\ &= \log \frac{\exp\left(-\frac{|\mathbf{y} - \mathbf{H}\mathbf{x}_i^0|^2}{2\sigma^2}\right)}{\exp\left(-\frac{|\mathbf{y} - \mathbf{H}\mathbf{x}_i^1|^2}{2\sigma^2}\right)}. \end{aligned} \quad (16)$$

Note that $\mathbf{y} = \mathbf{H}\mathbf{x} + \mathbf{n}$. We have

$$\mathbf{y} - \mathbf{H}\mathbf{x}_i^0 = \mathbf{H}[0, \dots, x_k - x_{k,i}^0, \dots, 0]^T + \mathbf{n} = \mathbf{h}_k(x_k - x_{k,i}^0) + \mathbf{n}.$$

Similarly, we have $\mathbf{y} - \mathbf{H}\mathbf{x}_i^1 = \mathbf{h}_k(x_k - x_{k,i}^1) + \mathbf{n}$, where the k th symbol in the transmitted symbol vector includes the i th bit, \mathbf{h}_k is the k th column of \mathbf{H} , and $x_{k,i}^0$ and $x_{k,i}^1$ are the symbols

that the i th bit has values of 0 and 1, respectively. Then, (16) can be written as

$$L_{M,e}(c_i) = \log \frac{\exp\left(-\frac{|\mathbf{h}_k(x_k - x_{k,i}^0) + \mathbf{n}|^2}{2\sigma^2}\right)}{\exp\left(-\frac{|\mathbf{h}_k(x_k - x_{k,i}^1) + \mathbf{n}|^2}{2\sigma^2}\right)}. \quad (17)$$

It can be observed that the equivalent channel is a SIMO channel

$$\mathbf{y}_k = \mathbf{h}_k x_k + \mathbf{n} \quad (18)$$

with only two possible input symbols $x_{k,i}^0$ and $x_{k,i}^1$.

As to the PIC-MMSE receiver, after the PIC stage, it is obvious from (4) that, if we assume perfect *a priori* information, the equivalent channel is also simplified to (18).

Next, we will show that the vector-APP detector (17) equals a scheme of MRC combining followed by a symbol-APP detector on the MRC output. Then, we will prove that MRC combining equals MMSE combining, therefore, the vector-APP demapper is equal to the PIC-MMSE demapper if we assume perfect *a priori* information.

For the channel output \mathbf{y}_k of (18), if we apply MRC combining, it is well known that the MRC weighting factor is just \mathbf{h}_k^H and the MRC output is given by $s_{k,\text{MRC}} = \mathbf{h}_k^H \cdot \mathbf{y}_k = |\mathbf{h}_k|^2 x_k + \mathbf{h}_k^H \cdot \mathbf{n}$, where $E[\mathbf{h}_k^H \cdot \mathbf{n}(\mathbf{h}_k^H \cdot \mathbf{n})^H] = |\mathbf{h}_k|^2 \cdot 2\sigma^2$. Therefore, the extrinsic information for the code bit i from the MRC output can be computed as

$$\begin{aligned} L_{\text{MRC},e}(c_i) &= \log \frac{\exp\left(-\frac{|s_{k,\text{MRC}} - |\mathbf{h}_k|^2 x_{k,i}^0|^2}{(|\mathbf{h}_k|^2 2\sigma^2)}\right)}{\exp\left(-\frac{|s_{k,\text{MRC}} - |\mathbf{h}_k|^2 x_{k,i}^1|^2}{(|\mathbf{h}_k|^2 2\sigma^2)}\right)} \\ &= \log \frac{\exp\left(-\frac{(|\mathbf{h}_k|^2 |x_k - x_{k,i}^0|^2 + 2\Re((x_k - x_{k,i}^0)(\mathbf{h}_k^H \cdot \mathbf{n})))}{(2\sigma^2)}\right)}{\exp\left(-\frac{(|\mathbf{h}_k|^2 |x_k - x_{k,i}^1|^2 + 2\Re((x_k - x_{k,i}^1)(\mathbf{h}_k^H \cdot \mathbf{n})))}{(2\sigma^2)}\right)}. \end{aligned} \quad (19)$$

It is easy to see that vector APP demapper output (17) equals the last step of (19). Therefore, these two detectors are equivalent.

On the other hand, if we apply MMSE combining to \mathbf{y}_k of (18), the MMSE vector can be computed as

$$\begin{aligned} w_k &= E[\mathbf{y}_k \mathbf{y}_k^H]^{-1} E[\mathbf{y}_k x_k^*] \\ &= (\mathbf{h}_k E|x_k|^2 \mathbf{h}_k^H + 2\sigma^2 \mathbf{I})^{-1} \mathbf{h}_k E|x_k|^2. \end{aligned}$$

Applying the matrix inversion lemma,⁵ we have

$$\begin{aligned} &(\mathbf{h}_k E|x_k|^2 \mathbf{h}_k^H + 2\sigma^2 \mathbf{I})^{-1} \\ &= \frac{1}{2\sigma^2} \mathbf{I} - \frac{1}{2\sigma^2} \mathbf{I} \mathbf{h}_k \left((E|x_k|^2)^{-1} + \frac{|\mathbf{h}_k|^2}{2\sigma^2} \right)^{-1} \mathbf{h}_k^H \frac{1}{2\sigma^2} \mathbf{I} \\ &= \frac{1}{2\sigma^2} \mathbf{I} - \frac{1}{2\sigma^2} \frac{\mathbf{h}_k \mathbf{h}_k^H}{2\sigma^2 (E|x_k|^2)^{-1} + |\mathbf{h}_k|^2}. \end{aligned}$$

⁵Matrix inversion lemma: If $\mathbf{A} = \mathbf{C} \mathbf{D}^{-1} \mathbf{C}^H + \mathbf{B}^{-1}$, $\mathbf{A}^{-1} = \mathbf{B} - \mathbf{B} \mathbf{C} (\mathbf{D} + \mathbf{C}^H \mathbf{B} \mathbf{C}) \mathbf{C}^H \mathbf{B}$.

Then, we have

$$\begin{aligned} w_k &= \frac{1}{2\sigma^2} E|x_k|^2 \mathbf{h}_k - \frac{1}{2\sigma^2} \frac{E|x_k|^2 |\mathbf{h}_k|^2 \mathbf{h}_k}{2\sigma^2 (E|x_k|^2)^{-1} + |\mathbf{h}_k|^2} \\ &= c \cdot \mathbf{h}_k \end{aligned}$$

where $c = (2\sigma^2 (E|x_k|^2)^{-1} + |\mathbf{h}_k|^2)^{-1}$ is a positive number. Then the MMSE combiner output is given as $s_{k,\text{MMSE}} = \mathbf{w}_k^H \cdot \mathbf{y}_k = c \cdot |\mathbf{h}_k|^2 x_k + c \cdot \mathbf{h}_k^H \cdot \mathbf{n}$, i.e., $s_{k,\text{MMSE}} = c \cdot s_{k,\text{MRC}}$. It is obvious then that $L_{\text{MMSE},e}(c_i) = L_{\text{MRC},e}(c_i)$.

Therefore, we proved that vector APP demapper is equal to PIC-MMSE demapper, assuming perfect *a priori* information.

ACKNOWLEDGMENT

The authors wish to thank the reviewers for many suggestions which helped to improve the quality of this paper. In particular, one reviewer suggested that we prove the results presented in the Appendix.

REFERENCES

- [1] I. E. Telatar, "Capacity of multiantenna Gaussian channels," *Eur. Trans. Telecommun.*, vol. 10, pp. 585–595, Nov. 1999.
- [2] A. M. Tonello, "Space-time bit-interleaved coded modulation with an iterative decoding strategy," in *Proc. IEEE Veh. Technol. Conf.*, Boston, MA, Sep. 2000, pp. 24–28.
- [3] M. Sellathurai and S. Haykin, "Turbo-blast for high-speed wireless communications," in *Proc. IEEE Wireless Commun. Networking Conf.*, Chicago, IL, Sep. 2000, pp. 315–320.
- [4] B. M. Hochwald and S. ten Brink, "Achieving near-capacity on a multiple-antenna channel," *IEEE Trans. Commun.*, vol. 51, no. 3, pp. 389–399, Mar. 2003.
- [5] A. Stefanov and T. M. Duman, "Turbo-coded modulation for systems with transmit and receive antenna diversity over block fading channels: System model, decoding approaches, and practical considerations," *IEEE J. Sel. Areas Commun.*, vol. 19, pp. 958–968, May 2001.
- [6] A. Reial and S. G. Wilson, "Concatenated space-time coding," in *Proc. Asilomar Conf. Signals, Syst., Computers*, vol. 1, Pacific Grove, CA, Nov. 2001, pp. 710–715.
- [7] J. Hagenauer. The turbo principle: Tutorial introduction and state of the art. presented at *Int. Symp. Turbo Codes, Related Topics*. [Online]. Available: <http://www.lnt.e-technik.tu-muenchen.de/veroefentlichungen/tut.ps.gz>
- [8] Y. Liu, M. P. Fitz, and O. Y. Takeshita, "Full rate space-time turbo codes," *IEEE J. Sel. Areas Commun.*, vol. 19, pp. 969–980, May 2001.
- [9] K. R. Narayanan, "Turbo decoding of concatenated space-time codes," in *Proc. 37th Annu. Allerton Conf. Commun., Control, Comput.*, Monticello, IL, Oct. 1999, pp. 217–226.
- [10] G. Bauch, "Concatenation of space-time block codes and "turbo"-TCM," in *Proc. IEEE Int. Conf. Commun.*, Vancouver, BC, Canada, Jun. 1999, pp. 1202–1206.
- [11] S. ten Brink, "Designing iterative decoding schemes with the extrinsic information transfer chart," *AEÜ Int. J. Electron. Commun.*, vol. 54, pp. 389–398, Nov. 2000.
- [12] —, "Exploiting the chain rule of mutual information for the design of iterative decoding schemes," in 39th Annu. Allerton Conf. Commun., Control, Comput., Oct. 2001.
- [13] S. ten Brink and B. M. Hochwald, "Detection thresholds of iterative MIMO processing," in *Proc. IEEE Int. Symp. Inf. Theory*, Lausanne, Switzerland, Jun. 2002, p. 22.
- [14] K. R. Narayanan and J. Li, "Bandwidth-efficient low-density parity-check coding using multi-level coding and iterative multi-stage decoding," in *Proc. 2nd Turbo Symp. Turbo Codes, Related Topics*, Brest, France, Jul. 2000, pp. 165–168.
- [15] G. Caire, D. Burshtein, and S. Shamai, "LDPC coding for interference mitigation at the transmitter," in 40th Annu. Allerton Conf. Commun., Control, Comput., Monticello, IL, Oct. 2002.

- [16] J. Hou, P. H. Siegel, L. B. Milstein, and H. D. Pfister, "Design of low-density parity-check codes for bandwidth-efficient modulation," in *Proc. IEEE Inf. Theory Workshop*, Cairns, Australia, Sep. 2001, pp. 24–26.
- [17] R. Narayanaswami, "Coded modulation with low density parity check codes," Master's thesis, Texas A&M Univ., College Station, TX, Jun. 2001.
- [18] J. Hou, P. H. Siegel, L. B. Milstein, and H. Pfister, "Capacity-approaching bandwidth-efficient coded modulation schemes based on low-density parity-check codes," *IEEE Trans. Inf. Theory*, vol. 49, pp. 2141–2155, Sep. 2003.
- [19] —, "Design of LDPC-coded MIMO systems with EXIT chart," in *Proc. 40th Annu. Allerton Conf. Commun., Control, Comput.*, Monticello, IL, Oct. 2002, pp. 227–236.
- [20] X. Wang and H. V. Poor, "Iterative (turbo) soft interference cancellation and decoding for coded CDMA," *IEEE Trans. Commun.*, vol. 47, pp. 1046–1061, Jul. 1999.
- [21] S. ten Brink, G. Kramer, and A. Ashikhmin, "Design of low-density parity-check codes for multi-input multi-output channels," in 40th Annu. Allerton Conf. Commun., Control, Comput., Monticello, IL, Oct. 2002.
- [22] M. Tüchler and J. Hagenauer, "Exit charts and irregular codes," in *Proc. Conf. Inf. Sci. Syst.*, Princeton, NJ, Mar. 2002, pp. 748–753.
- [23] S. M. Alamouti, "A simple transmit diversity technique for wireless communications," *IEEE Trans. Commun.*, vol. 16, no. 10, pp. 1451–1458, Oct. 1998.
- [24] V. Tarokh, H. Jafarkhani, and A. R. Calderbank, "Space-time block codes from orthogonal designs," *IEEE Trans. Inf. Theory*, vol. 45, no. 5, pp. 1456–1467, May 1999.
- [25] G. Bauch and J. Hagenauer, "Smart versus dumb antennas—Capacities and FEC performance," *IEEE Commun. Lett.*, vol. 6, pp. 55–57, Feb. 2002.
- [26] G. Bauch, "Introduction to multiantenna systems and space-time codes," in *Proc. 3rd Int. Workshop Commercial Radio Sensors, Commun. Tech.*, Linz, Austria, Aug. 2001, pp. 50–56.
- [27] T. J. Richardson, M. A. Shokrollahi, and R. L. Urbanke, "Design of capacity-approaching irregular low-density parity-check codes," *IEEE Trans. Inf. Theory*, vol. 27, pp. 619–637, Jan. 2001.
- [28] J. H. Winters, "On the capacity of radio communication systems with diversity in a Rayleigh fading environment," *IEEE J. Sel. Areas Commun.*, vol. SAC-5, no. 5, pp. 871–878, May 1987.
- [29] R. A. Horn and C. R. Johnson, *Matrix Analysis*. Cambridge, U.K.: Cambridge Univ. Press, 1985.
- [30] U. Wachsmann, R. F. H. Fischer, and J. B. Huber, "Multilevel codes: Theoretical concepts and practical design rules," *IEEE Trans. Inf. Theory*, vol. 45, pp. 1361–1391, Jul. 1999.
- [31] B. Hassibi and B. M. Hochwald, "High-rate codes that are linear in space and time," *IEEE Trans. Inf. Theory*, vol. 48, pp. 1804–1824, Jul. 2002.

Jilei Hou (S'00–M'04) received the B.E. degree (with highest honors) and the M.E. degree in radio engineering from Southeast University, Nanjing, China, in 1995 and 1998, respectively, and the Ph.D. degree in electrical engineering from the University of California, San Diego, La Jolla, CA, in 2003.

He is currently with the Corporate R&D Group, Qualcomm Inc., San Diego, CA, where he is involved in the design of the next generation high-speed wireless communication systems. His research interests include communication theory, information theory, channel coding, spread spectrum, and space-time communications.



Paul H. Siegel (M'82–SM'90–F'97) received the S.B. degree in mathematics in 1975 and the Ph.D. degree in mathematics in 1979, both from the Massachusetts Institute of Technology (MIT), Cambridge.

He held a Chaim Weizmann Postdoctoral Fellowship at the Courant Institute, New York University. He was with the IBM Research Division in San Jose, CA, from 1980 to 1995. He joined the faculty of the School of Engineering at the University of California, San Diego in July 1995, where he is currently Professor of Electrical and Computer Engineering. He is

affiliated with the California Institute of Telecommunications and Information Technology, the Center for Wireless Communications, and the Center for Magnetic Recording Research where he currently serves as Director. His primary research interests lie in the areas of information theory and communications, particularly coding and modulation techniques, with applications to digital data storage and transmission.

Prof. Siegel was a member of the Board of Governors of the IEEE Information Theory Society from 1991 to 1996. He served as co-Guest Editor of the May 1991 Special Issue on Coding for Storage Devices of the IEEE TRANSACTIONS ON INFORMATION THEORY, served the same Transactions as Associate Editor for Coding Techniques from 1992 to 1995, and as Editor-in-Chief from 2001 to 2004. He was also Co-Guest Editor of the May/September 2001 two-part issue on The Turbo Principle: From Theory to Practice of the IEEE JOURNAL ON SELECTED AREAS IN COMMUNICATIONS. He was co-recipient, with R. Karabed, of the 1992 IEEE Information Theory Society Paper Award and shared the 1993 IEEE Communications Society Leonard G. Abraham Prize Paper Award with B. Marcus and J. K. Wolf. He holds 17 patents in the area of coding and detection, and was named a Master Inventor at IBM Research in 1994. He is also a member of Phi Beta Kappa.



Laurence B. Milstein (S'66–M'68–SM'77–F'85) received the B.E.E. degree from the City College of New York, New York, NY, in 1964, and the M.S. and Ph.D. degrees in electrical engineering from the Polytechnic Institute of Brooklyn, Brooklyn, NY, in 1966 and 1968, respectively.

From 1968 to 1974, he was with the Space and Communications Group of Hughes Aircraft Company, and from 1974 to 1976, he was a member of the Department of Electrical and Systems Engineering, Rensselaer Polytechnic Institute, Troy, NY. Since

1976, he has been with the Department of Electrical and Computer Engineering, University of California at San Diego, La Jolla, where he is a Professor and former Department Chairman, working in the area of digital communication theory with special emphasis on spread-spectrum communication systems. He has also been a consultant to both government and industry in the areas of radar and communications.

Dr. Milstein was an Associate Editor for Communication Theory for the IEEE TRANSACTIONS ON COMMUNICATIONS, an Associate Editor for Book Reviews for the IEEE TRANSACTIONS ON INFORMATION THEORY, an Associate Technical Editor for the *IEEE Communications Magazine*, and the Editor-in-Chief of the IEEE JOURNAL ON SELECTED AREAS IN COMMUNICATIONS. He was the Vice President for Technical Affairs in 1990 and 1991 of the IEEE Communications Society, and has been a member of the Board of Governors of both the IEEE Communications Society and the IEEE Information Theory Society. He is a former Chair of the IEEE Fellows Selection Committee, and a former Chair of ComSoc's Strategic Planning Committee. He is a recipient of the 1998 Military Communications Conference Long Term Technical Achievement Award, an Academic Senate 1999 UCSD Distinguished Teaching Award, an IEEE Third Millennium Medal in 2000, the 2000 IEEE Communication Society Armstrong Technical Achievement Award, and the 2002 MILCOM Fred Ellersick Award.